

## Acoustic emission monitoring of damage progression in CFRP retrofitted RC beams

Archana Nair<sup>a</sup>, C.S. Cai<sup>\*</sup>, Fang Pan<sup>b</sup> and Xuan Kong<sup>c</sup>

Department of Civil and Environmental Engineering, Louisiana State University, Baton Rouge, LA, 70803, USA

(Received January 30, 2014, Revised March 20, 2014, Accepted March 21, 2014)

**Abstract.** The increased use of carbon fiber reinforced polymer (CFRP) in retrofitting reinforced concrete (RC) members has led to the need to develop non-destructive techniques that can monitor and characterize the unique damage mechanisms exhibited by such structural systems. This paper presented the damage characterization results of six CFRP retrofitted RC beam specimens tested in the laboratory and monitored using acoustic emission (AE). The focus of this study was to continuously monitor the change in AE parameters and analyze them both qualitatively and quantitatively, when brittle failure modes such as debonding occur in these beams. Although deterioration of structural integrity was traceable and can be quantified by monitoring the AE data, individual failure mode characteristics could not be identified due to the complexity of the system failure modes. In all, AE was an effective non-destructive monitoring tool that can trace the failure progression in RC beams retrofitted with CFRP. It would be advantageous to isolate signals originating from the CFRP and concrete, leading to a more clear understanding of the progression of the brittle damage mechanism involved in such a structural system. For practical applications, future studies should focus on spectral analysis of AE data from broadband sensors and automated pattern recognition tools to classify and better correlate AE parameters to failure modes observed.

**Keywords:** acoustic emission; reinforced concrete; CFRP; intensity analysis

---

### 1. Introduction

Retrofitting reinforced concrete (RC) structures using materials such as fiber reinforced polymers (FRP) has gained popularity in the past decades. This has been mainly due to the maintenance and repair requirements of existing civil infrastructure and the versatile features of FRP composites, such as light weight, ease in onsite application, good corrosion resistance, etc. However, for RC beams externally retrofitted with FRP the debonding failure mechanism has been deemed the most critical failure mode (Teng *et al.* 2001). There have been numerous efforts to counter this form of failures, yet the complex nature of this failure mechanism has not led to convincing mitigation solutions. Thus, there is a genuine need for a real time non-destructive

---

\*Corresponding author, Edwin B. and Norma S. McNeil Distinguished Professor, E-mail: [cscail@lsu.edu](mailto:cscail@lsu.edu)

<sup>a</sup> Research Assistant

<sup>b</sup> Research Assistant

<sup>c</sup> Research Assistant

monitoring system that can assess the structural integrity of such a structural system where the failure modes are more complex than regular reinforced concrete structures.

Non-destructive techniques used for debonding detection to date are comprised of numerous methods such as acoustic emission (AE) (Mirmiran *et al.* 1999), ultrasonic pulse velocities (UPV) (Mirmiran and Wei 2001), infrared thermography (Levar and Hamilton 2003), fiber optic sensing (FOS) (Whitten *et al.* 1999, Lau *et al.* 2001, Casas *et al.* 2002, Ansari 2005), etc. These techniques are shown to successfully identify FRP debonding in specimens tested in controlled laboratory environments. Yet, the application of these techniques for continuous monitoring of existing structures requires validation.

Very limited literature is available with regards to research carried out using AE for debonding detection in FRP retrofitted RC structures. One of the first attempts was made by Henkel and Wood (1991). They studied cumulative AE parameters to characterize cracking behavior in retrofitted RC beams with bonded plates made of varied materials including FRP. AE event location and tracking AE parameter characteristics during failure progression of RC beams retrofitted with carbon laminates was the focus of studies conducted by Johnson *et al.* (2001) and Park *et al.* (2004). In 2006, Ridge and Ziehl (2006) compared an AE evaluation criterion with the criterion developed from the cyclic load test method to assess the structural integrity of strengthened RC beams. The results obtained, though credible, were from a limited number of specimens and thus could not be generalized. A recent study conducted by Degala *et al.* (2008) concluded that monitoring the damage initiation, progression, and location using AE is possible in concrete slab specimens strengthened with FRP strips.

This paper presents the performance results of six FRP retrofitted RC beams that were subjected to monotonically increasing loads to failure and monitored continuously using AE. The typical load profile of testing consisted of load holds, except two beams that were subjected to additional load drops and rises to assess the existence of Kaiser effect. Damage evaluation was done by both parametric and intensity analysis techniques.

## 2. Theoretical background

AE is the class of phenomena whereby transient elastic waves are generated by the rapid release of energy from a localized source or sources within a material, or the transient elastic wave(s) so generated (ASTM E1316-07b 2007). In short, a developing flaw emits bursts of energy in the form of high frequency sound waves that propagate within the material and are received by piezoelectric sensors.

Both RC and FRP materials are materials that emit discrete bursts of energy when subjected to increasing loads. Types of damages that typically form AE sources in concrete are micro cracking, corrosion of reinforcing steel, etc. (Ghorbanpoor and Rentmeester 1993, Yuyama *et al.* 1999), while typical damage modes from FRP are delamination, matrix cracking, yielding of tensile face sheets, debonding, and fiber breakage (Mirmiran and Philip 2000, Cecchini 2005). Failures of FRP strengthened RC flexural members may take place through several mechanisms such as steel yielding followed by FRP rupture, shear failure of concrete, cover delamination, FRP debonding, etc. (Buyukozturk and Hearing 1998). Again, there exist possibilities for several types of debonding in FRP strengthened RC members that can occur at different interfaces of such structures (Buyukozturk *et al.* 2004). The debonding mechanism is the AE source of interest in monitoring retrofitted RC beams in this study.

Typically, AE signals collected can be represented by characteristic parameters such as amplitude, duration, etc., and are qualitatively evaluated using these parameters. There are numerous qualitative as well as quantitative ways to interpret these signal parameters or waveforms. Parametric analysis of AE signals resulted in for example: (i) Concrete beam integrity (CBI) ratio that is defined as a ratio of the load at onset of AE to the maximum prior load (Yuyama *et al.* 1999) and (ii) Calm and Load ratios of reinforced concrete beams; where the calm ratio is the cumulative AE activities during the unloading process to those up to the last maximum loading and the load ratio is between the load at onset of AE to the prior load (Ohtsu *et al.* 2002). Meanwhile, quantification by statistical analysis of parameters gave rise to the use of Historic and Severity indices in assessing RC structural members (Golaski *et al.* 2002). This intensity analysis technique had already been successfully applied to FRP and metal piping system evaluations (CARP 1987).

Here, the damage progression trends of the six reinforced concrete beams that are retrofitted with carbon FRP (CFRP) laminates and tested under quasi-static loading conditions are discussed. The intensity analysis technique involves the use of two values known as Historic index and Severity. They are derived from the signal strength data recorded during a test using the following formulas (Fowler *et al.* 1992)

$$H(t) = \frac{N}{N-K} \cdot \left( \frac{\sum_{i=K+1}^N S_{oi}}{\sum_{i=1}^N S_{oi}} \right) \quad (1)$$

$$S_r = \frac{1}{J} \cdot \left( \sum_{m=1}^J S_{om} \right) \quad (2)$$

where  $H(t)$  – Historic index;  $N$  – number of hits up to time  $t$ ;  
 $S_{oi}$  – signal strength of the  $i^{\text{th}}$  hit;  $K$  – empirically derived constant based on material;  
 $S_r$  – Severity  $J$  – empirically derived constant based on material;  
 $S_{om}$  – signal strength of the  $m^{\text{th}}$  hit, where the order of  $m$  is based on signal strength magnitude.

In the present study for concrete,  $K$  values are related to  $N$  by:  $N \leq 50$ ,  $K = 0$ ;  $51 \leq N \leq 200$ ,  $K = N - 30$ ;  $201 \leq N \leq 500$ ,  $K = 0.85 N$ ;  $N \geq 501$ ,  $K = N - 75$  and  $J$  values for  $N < 50$ ,  $J = 0$ ;  $N \geq 50$ ,  $J = 50$ . (Chotickai 2001, Golaski *et al.* 2002). For CFRP,  $K$  values are related to  $N$  by:  $101 \leq N \leq 500$ ,  $K = 0.8N$ ; and for  $N > 500$ ,  $K = N - 100$ , and  $J$  values for  $N < 20$ ,  $J = 0$ ;  $N \geq 20$ ,  $J = 20$  (Fowler *et al.* 1992).

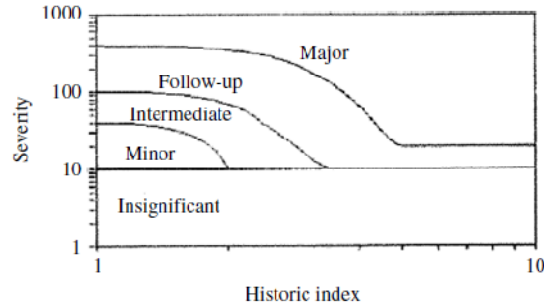


Fig. 1 Typical intensity chart for FRP material

The historic index is an analytical quantity that traces the slope change of the cumulative signal strength parameter measured during a test. A knee in the cumulative signal strength vs. time graph is usually a representative of new damage. This can be easily identified by determining the historic index as the value peaks at every AE knee and generally tend to decrease until the next AE knee. While determining the historic index it is important to be aware that the technique is not suitable for the situation with few hits as it may fluctuate considerably when dealing with a small data set. The other value required for intensity charts is Severity. This value is obtained by averaging the strongest signal strength values and helps normalize the collected AE data making it independent of the location of the AE source. When assessed over successive cycles of loading, the severity increases or remains steady based on the amount of damage that has taken place within the specimen (Gostautas *et al.* 2005). The intensity chart shown in Fig. 1 is a typical chart on which maximum values of historic index and severity are plotted to determine the intensity of a source (CARP 1987).

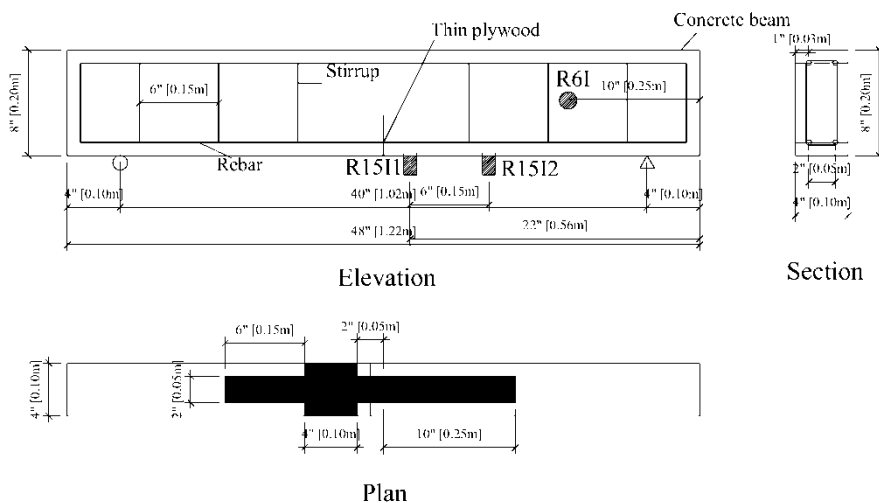


Fig. 2 Beam specimen details

### 3. Experimental program

#### 3.1 Beam specimen details

A total of ten reinforced concrete beams were fabricated in the Louisiana Transportation Research Center (LTRC) and Louisiana State University (LSU) concrete lab facility. Each of the beams was externally bonded with CFRP material as shown in Fig. 2. Although all beams were subjected to flexural loading, only six of the ten beams were monitored using acoustic emission. All the beams were constructed in a similar way, whose typical details of construction and dimensions are represented in Fig. 2.

The beams are 1.220 m (4 ft) long with a cross sectional dimension of 102x203 mm (4"x8"). The average compressive strength of concrete is 30MPa. The reinforcements consisted of four longitudinally placed #3 mild steel bars and shear reinforcement consisted of #3 stirrups spaced 152 mm (6") apart. The yield strength of the bars was 420MPa. A thin wooden piece (Fig. 2) was inserted at the midspan to initiate cracks and debonding at this location. At the soffit of the beams a 559 x 51 mm (22"x2") CFRP strip was bonded with a two-part epoxy purchased from Sika Corporation. The strip was vertically wrapped on one side to force the debonding to occur on the other side.

#### 3.2 Testing arrangement

Each test consisted of flexural loading on the beam with a loading actuator controlled by a MTS controller. Each beam was sequentially designated as SD1, SD2, SD3, SS1, SS2, and SM1. In the naming the letter 'S' stands for specimen, 'D' for delamination mode of failure, the second 'S' for shear mode of failure, and 'M' stands for a mixed mode failure. The numbers help to sequentially identify the number of samples that were observed to fail in a particular mode. The load transfer mechanisms adopted for each beam test case is shown in Figs. 3(a), - 3(c).

All beams were setup for a three-point bending arrangement. Between the load transfer mechanisms and the load point of the beam, 1/8 inch thick rubber pads were placed to reduce background noise emissions that may contaminate acoustic source data. The loading was controlled using a MTS Flex system with a capacity of 489 kN (110 kips) in compression force. Load control was used for all the beam tests.

The AE system used for acquisition is from Physical Acoustics Corporation (PAC). Two resonant piezoelectric transducers with integral preamplifiers, R15I (150 kHz) and R6I (60 kHz) bandpassed from 100 kHz to 300 kHz and 20 kHz to 150 kHz, respectively, were used for monitoring AE activities in all beams. The beam specimen SD1 was instrumented with two R15I transducers. While the R6I was placed on the concrete surface close to the end where delamination of the CFRP strip was expected, the R15I sensor was placed on the composite layer close to the mid-span region of the beam to acquire sources originating close to the artificially introduced crack (Fig. 2). All R15I sensors located on the laminate surface were removed at load levels close to 80% of the ultimate load (UL) to avoid debonding caused damage to the sensors. Various other sensors such as external strain gages, deflection gauges, and fiber optic sensors were also attached to the specimen to monitor damage progression, which limits the space to attach more AE sensors in the damage region of interest.

Prior to conducting any actual AE monitoring it is essential to check the sensitivity and coupling properties of the sensor to the specimen. For this, a pencil lead break (PLB) test similar

to that recommended by ASTM E 2075 was carried out before and after each test. The procedure basically consists of breaking 0.3-0.5 mm pencil leads of 2.5 mm length at a 30 degree orientation to the surface and the amplitudes recorded at a given sensor are measured at different time intervals to ensure that the sensitivity at the sensor does not vary by more than 3dB.

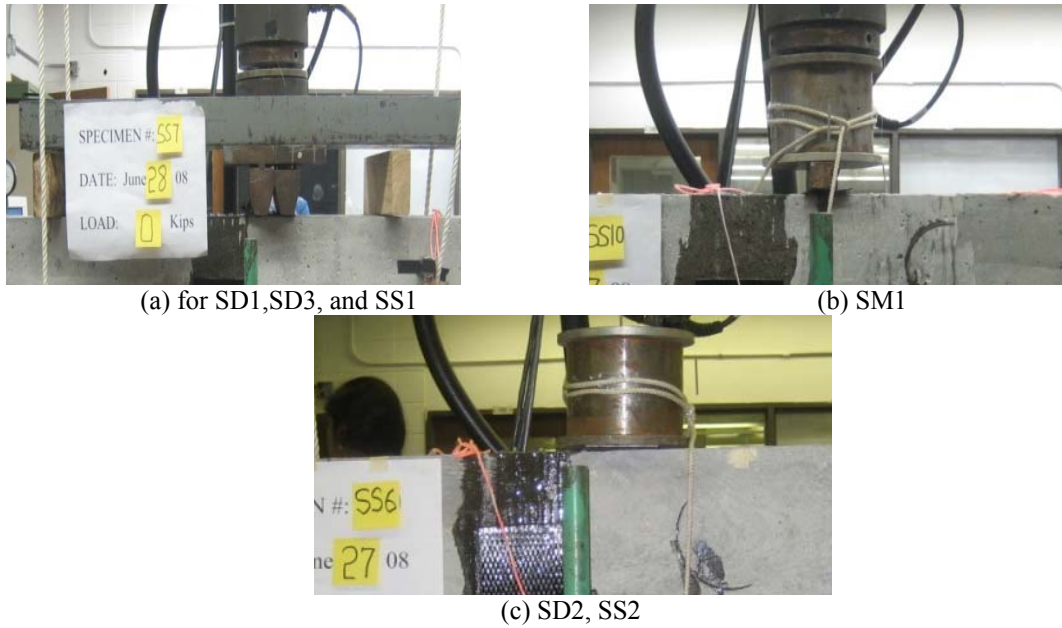


Fig. 3 Load transfer mechanisms

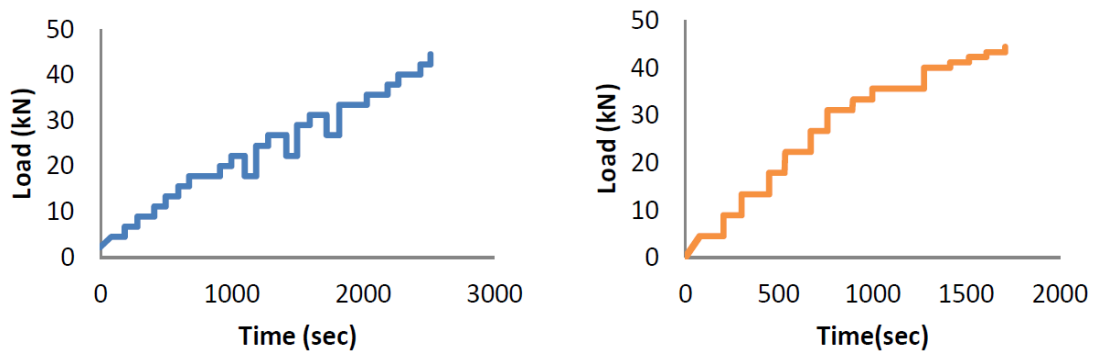


Fig. 4 (a) Load profile for beams SD1 and SS1 and (b) Load profile for all other beams

### 3.3 Loading schedule

While the load schedule for beams SD1 and SS1 was a step loading including unloading phases

as shown in Fig. 4(a), all other beams were subjected to monotonically increasing loads with load hold periods of approximate 2-5 minutes. The hold periods after each load step facilitated the timely recording of strain, deflection and visual observations of cracks at each load step. A typical load profile for all subsequent beams is shown in Fig. 4(b).

### 3.4 Instrumentation setup

Certain parameters need to be set in the acquisition system before testing, based on material being tested and the background noise level. Since in this study reinforced concrete beam specimens with external CFRP reinforcement were used, the following PAC recommended instrument settings shown in Table 1 were made to capture adequate damage related acoustic signals. Acquisition threshold is a part of standard hardware setup that sets the detection threshold for the acquisition system, enabling reduction of background noise in the recorded data. HDT, PDT and HLT are all timing parameters of the signal acquisition process and have material specific values. HDT sets the extent of a signal to be accounted as one hit, PDT ensures the exact identification of signal peak and a proper HLT setting enables discarding of spurious signal decay measurements.

Table 1 Acquisition instrument setup values

Parameter	Set value (R6I)	Set value (R15I)
Acquisition threshold	45 dB	45 dB
Hit definition time (HDT)	50 $\mu$ s	200 $\mu$ s
Peak definition time (PDT)	800 $\mu$ s	400 $\mu$ s
Hit lock out time (HLT)	1000 $\mu$ s	1000 $\mu$ s

## 4. Test results

The results obtained from analyzing the AE data of the six tested beams are discussed in this section. A summary of the failure loads and maximum intensity values are shown in Table 2. A detailed discussion of the parametric and intensity analyses results obtained for each representative test case is followed.

Table 2 Summary of results

Beam specimen	Failure load (kN)	H(t)-Sr (Max)	
		R15I	R6I
SD1	47.818	25.8294 – 20.1	-
SD2	45.594	35.4584 – 15.974	202.958 – 141.618
SD3	48.930	15.2848 – 7.7375	90.2346 – 104.576
SS1	46.706	2.5218 – 4.92	8.5535 – 7.11
SS2	48.930	9.836 – 10.1235	184.311 – 232.362
SM1	44.482	20.9676 – 8.615	-

#### 4.1 Test case 1: Beam specimens SD1, SD2 and SD3

The scatter plot of AE hit amplitude vs. time of the beam SD1 (Fig. 5), consists of AE hits recorded from two R15I sensors located on the CFRP laminate surface of the beam. Time marks that represent each new load step in the loading schedule are clearly visible as vertical lines in these scatter plots. During the first 5 minutes of loading it can be noticed that relatively very few AE events were generated. At this stage, there were also no visible cracks. From about 20% of the UL, high AE activity was visible at every new load step. Although no cracks were externally visible, the flexural crack artificially induced at the midspan might have gradually begun to widen causing high energy AE signals to be generated at each load step. Gostautas *et al.* (2005) also reported similar high activity at low level loads in FRP composite bridge deck panels and attributed this to the presence of excess resin. Since an epoxy resin system was also used in attaching the CFRP to the RC beams in this study, the same can be assumed to contribute to the anomalous AE activity observed. The number of high amplitude events steadily rise as flexural cracks initiate and propagate.

There were three loading /unloading sequences at 38% (18.17 kN), 57% (27.26 kN) and 66% (31.56 kN) of UL, respectively, with 2-minute load holds shown in Fig. 4(a). During these loading sequences no emissions were recorded, which is represented in the clean area of Fig. 5 around time intervals 697-781s, 1215-1327s and 1648-1727s. Thus, these clean regions in the graph validate the presence of the Kaiser effect in these retrofitted beams, confirming that no permanent damage had occurred until this phase of loading. The Kaiser effect, an AE signature characteristic, states that a material under loading emits acoustic emissions only after a primary load level is exceeded. Acoustic activity will be absent in the unloading phase.

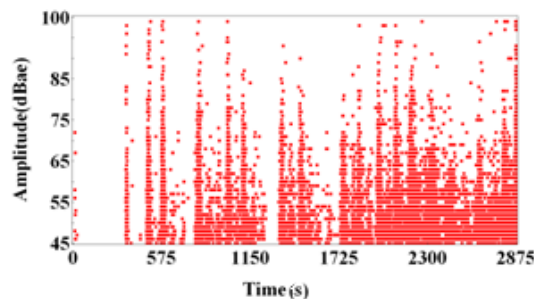


Fig. 5 Beam SD1: Amplitude vs time

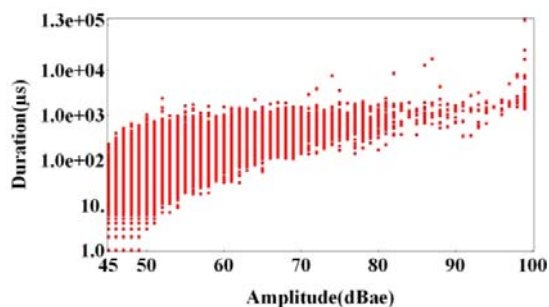


Fig. 6 Beam SD1: Amplitude vs Duration

Amplitude versus duration plots have been recommended by CARP (1987) to assess the quality of AE data. Genuine AE data generally creates a banded plot while the non-genuine hits such as those caused by mechanical rubbing and electromagnetic interference (EMI) appear in the area outside the band (Fowler *et al.* 1989). The trend seen in Fig. 6 clearly illustrates that the plot is well banded with very few non-AE source hits, confirming that all collected data are from the monitored structure. Another AE correlation plot generated for this beam was the signal strength vs. duration plot shown in Fig. 7. During testing along with the acquisition of standard AE parameters, waveforms were also collected. This leads to the observation of the occurrence of certain single AE events close to the failure load that actually consisted of two closely spaced hits. A typical waveform collected at loads close to failure is illustrated in Fig. 8. Thus, if these double hits were represented appropriately in the amplitude distribution plot (Fig. 5), the plot would have been denser close to failure load with more high amplitude hits, which is expected as loads increase.

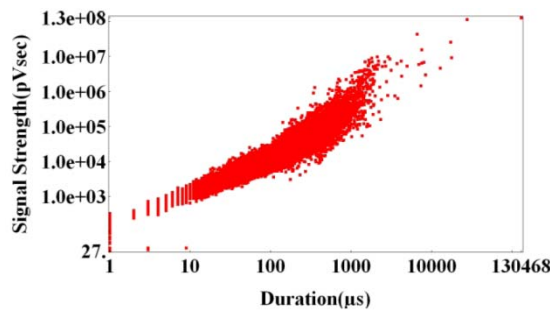


Fig. 7 Beam SD1: Signal strength vs Duration

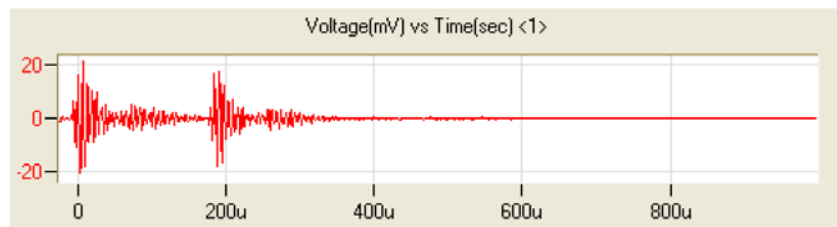


Fig. 8 Double hit AE signal waveform

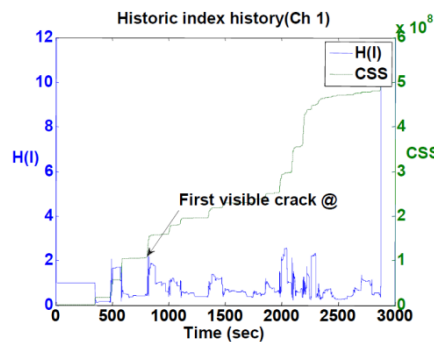


Fig. 9 Beam SD1: H(I)-CSS plot for R15I sensor located close to center of beam

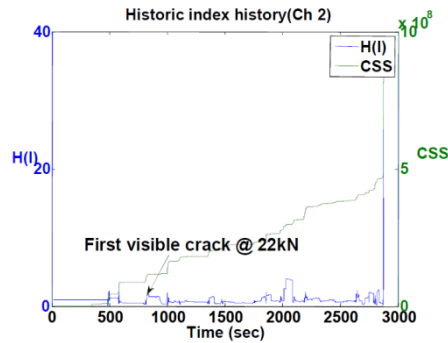


Fig. 10 Beam SD1: H(I)-CSS plot for R151 sensor located close to end of FRP strip

To quantitatively assess the progression of damage in the retrofitted beams the intensity analysis has also been conducted. As discussed earlier, the historic index is an analytical quantity that traces the slope change of the cumulative signal strength parameter measured during a test. A knee in the cumulative signal strength vs. time graph is usually a representative of new damage. Historic index  $H(I)$  values plotted along with the cumulative signal strength (CSS) profiles are clear identifiers of the onset of new damage as seen in Figs. 9 and 10. In the historic index profile it is clearly visible that each increasing load step that causes a rise in the cumulative signal strength can correspondingly be matched with a spike in the  $H(I)$  value. On reviewing these figures with visual observations and correlation plots (Figs. 5-7), it can be confirmed that permanent damage occurred before the third unloading sequence commenced. It is noted that the actual first crack may have occurred earlier than the first observed crack as marked on these figures.

The maximum values of historic and severity indices obtained at each load step for this beam from both AE channels are represented in Fig. 11. The typical trend, namely, the intensity values of higher damage significance plotting toward the top right-hand corner of the chart and values of lesser significance near the bottom left, can also be observed in Fig. 11. Thus, channel 2 located close to the CFRP strip end seemed to have collected stronger signals conducive to the visual observations of the absence of any flexural cracks in this region, which in turn provides continuous media for the AE waves to reach the sensor with less attenuation.

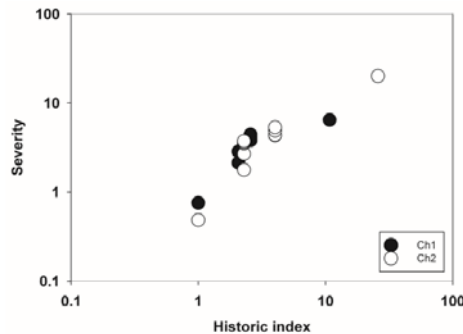
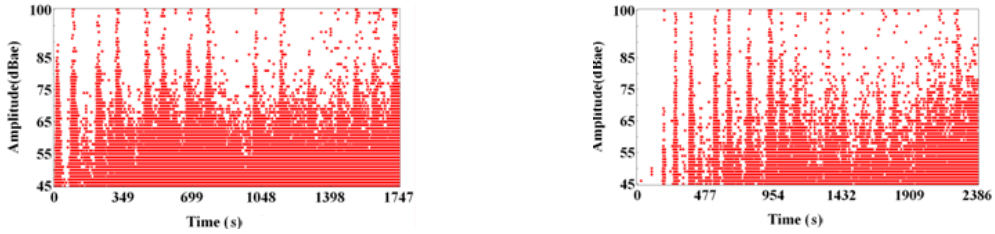
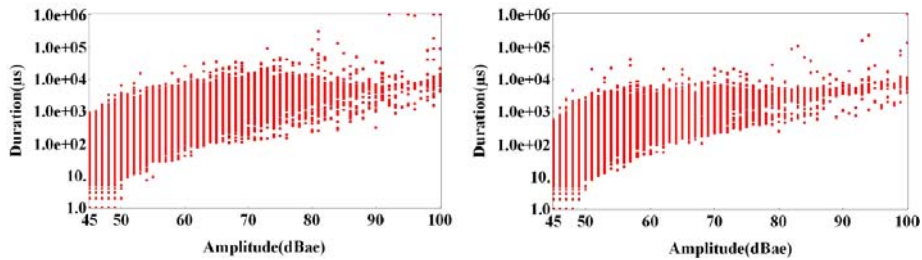


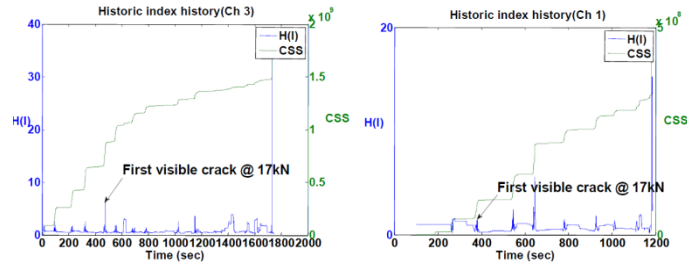
Fig. 11 Intensity chart for Beam SD1



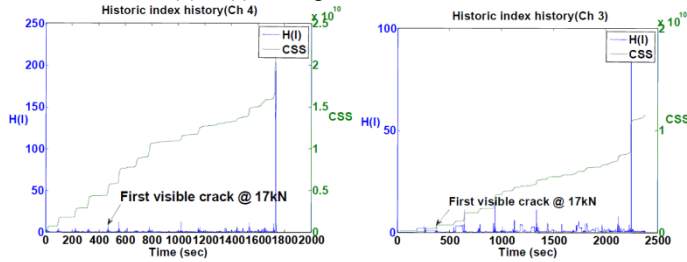
(a) Amplitude vs time



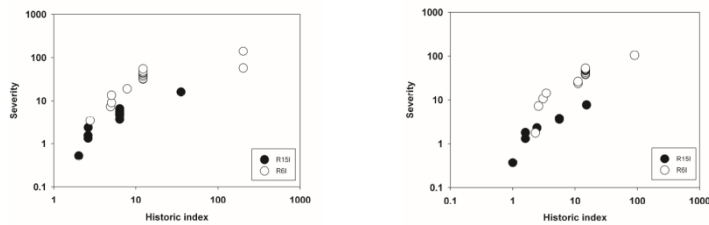
(b) Amplitude vs Duration



(c) H(I)-CSS plot for R15I sensor



(d) H(I)-CSS plot for R6I sensor



(e) Intensity charts

Beam SD2 (left part)

Beam SD3 (right part)

Fig. 12 Parametric and intensity results of beams SD2 and SD3

On the whole, the first visually observable flexural crack was located in the midspan at 22 kN load (46% of UL). More flexural cracks were observed at the soffit of the beam from 31 kN load (65% of UL) onwards. Ultimately, the beam failed at 47.818 kN load by delamination of the CFRP strip from the end with the concrete cover removal at regions close to the center. These observations are clearly indicated in the intensity chart as the sensor (Ch2) located at the end of the laminate recorded more events than sensor Ch1.

The trends observed in parametric and intensity results from beams SD2 and SD3 that failed by delamination mode was similar to that observed in beam SD1 and are shown in Fig. 12. It must be noted from here on that all results shown are from two different resonant AE sensors, a R6I sensor placed on the concrete surface and a R15I sensor placed on the CFRP laminate surface close to the center of the beam.

#### 4.2 Test case 2: Beam specimen SS1

This beam was also tested under similar conditions and was subjected to step loading as mentioned earlier. However, the failure mode seen in this particular beam was unexpected and happened due to shear across the unretrofitted portion of the beam. A general examination of the amplitude history plot clearly shows increasing amplitude for increased loads, but the AE activity was much weaker in comparison to all other beams tested as the AE sources were away from the sensing proximity of the sensors. In spite of the weaker signal amplitudes the Kaiser effect is still visible at early load levels in Fig. 13 at time intervals of 1100-1190s, 1424-1498s and 1658-1732s. Similarly, the amplitude vs. duration plot also shows very few presence of non-genuine AE hits in Fig. 14.

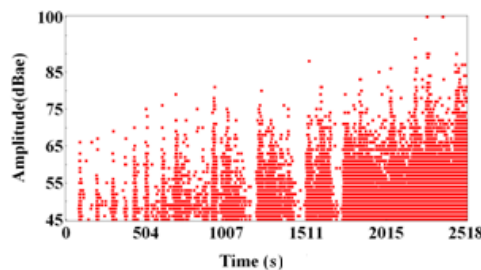


Fig. 13 Beam SS1: Amplitude vs time

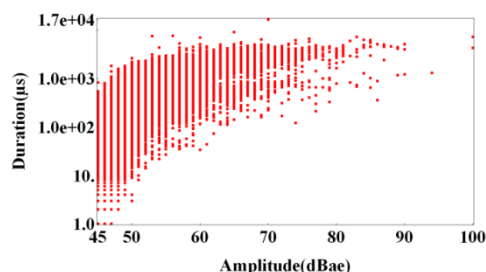


Fig. 14 Beam SS1: Amplitude vs Duration

Again, visually recognized patterns in the correlation plots are validated quantitatively by the intensity results. As stated earlier, two different resonant sensors were used for this test case with the R6I sensor placed on the concrete surface and the R15I sensor placed close to the center of the beam on the FRP laminate surface. Both historic index plots (Figs. 15 and 16) for sensors R6I and R15I clearly reveal low historic index values, which correlates well with the visually observed form of damage. This beam developed cracks away from the direction of CFRP reinforcement and failed due to a shear crack developed in the beam, resulting in weak signals in the AE monitored zone. Significant rise in slope of the CSS curve is again observable in both historic index plots from about 80% of the ultimate load indicative of significant damage presence at that loading level. Intensity chart trends also progress as expected, with historic and severity indices gradually increasing in value from 1 -10 (Fig. 17).

This beam unexpectedly began failing in shear when the load was about 80% of the ultimate load and failed at 46.706 kN. Both the progression of failure and the location of damage are traceable with the AE data recorded, since weaker signals represent a distant source and yet provide ample warning before the beam actually failed.

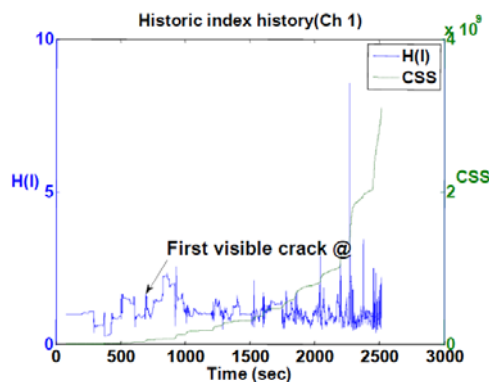


Fig. 15 Beam SS1: H(I)-CSS plot for R6I sensor

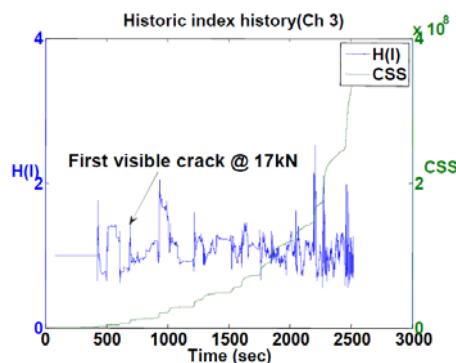


Fig. 16 Beam SS1: H(I)-CSS plot for R15I sensor

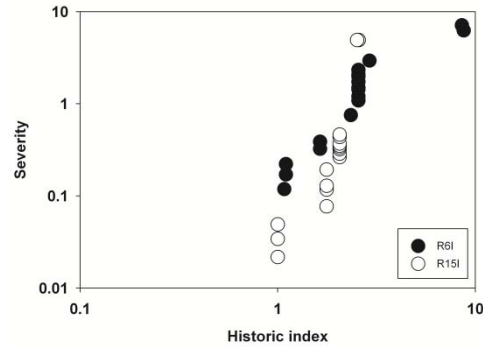


Fig. 17 Intensity chart for beam SS1

#### 4.3 Test case 3: Beam specimen SS2

The result plots generated for this beam specimen has similar trends to plots obtained in previous test cases. Copious amounts of AE data were collected with relatively greater proportion of high amplitude signals (Fig. 18). The typical banded pattern is also clearly visible in Fig. 19, confirming absence of non-genuine AE data. The historic index profiles for both sensors are shown in Figs. 20 and 21. Again, the lower historic index values were collected from the sensor located on the laminate surface (R15I). This trend confirms with the actual mode of failure observed at this beam, which consisted of shear failure induced delamination. The high value peaks indicate development of new cracks. The intensity chart trends (Fig. 22) are also in conformance with expectations. Even in the AE sensor located on the concrete surface the low severity values indicate the presence of a widening crack in the concrete cross-section that resulted in attenuation of the collected signals. The beam ultimately failed at 48.93 kN load.

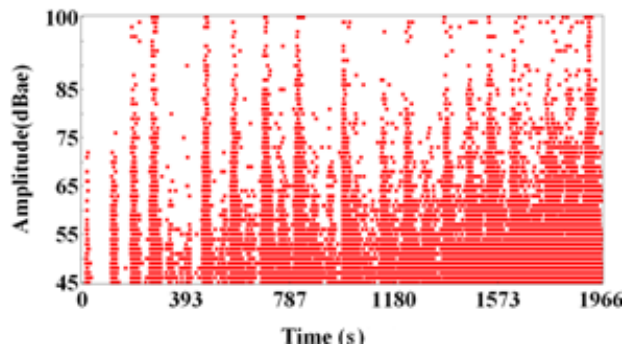


Fig. 18 Beam SS2: Amplitude vs time

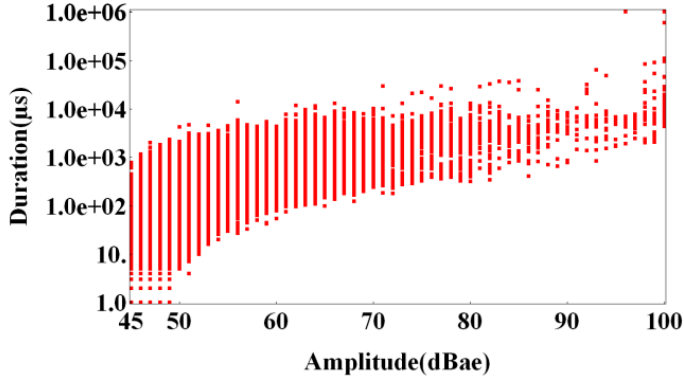


Fig. 19 Beam SS2: Amplitude vs Duration

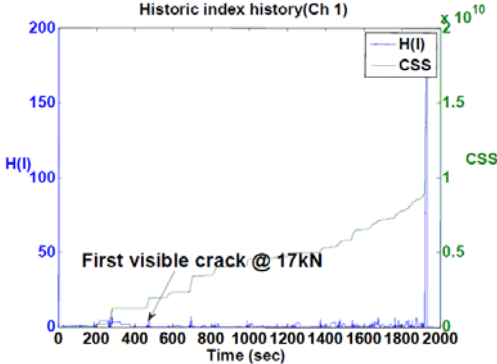


Fig. 20 Beam SS2: H(I)-CSS plot for R6I sensor

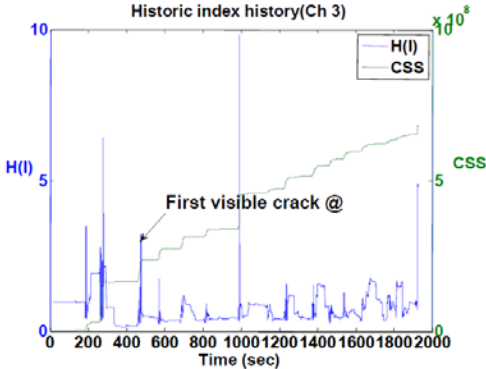


Fig. 21 Beam SS2: H(I)-CSS plot for R15I sensor

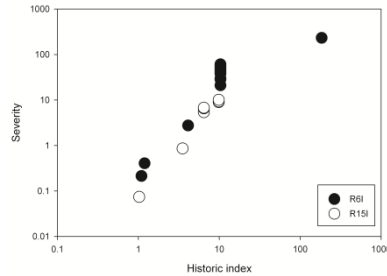


Fig. 22 Intensity chart for Beam SS2

#### 4.4 Test case 4: Beam specimen SM1

Although the testing and analysis followed for this beam was similar to previously discussed cases, the failure mode of SM1 was unique. This beam showed initiation cracks at the soffit of the beam and the flexural crack growth continued until 90% of the UL. Although both R6I and R15I sensors were used for AE monitoring of this beam, the R6I sensor malfunctioned during testing, thus, no AE data was obtained from this channel. The only functional AE sensor (R15I) was removed before the beam failure to prevent damages to the sensor. The observed failure was sudden and may be categorized as a mixed mode of debonding, which began with crushing of concrete at the load point and followed by shear crack induced interfacial debonding of CFRP laminate.

From the trends observed in the AE amplitude history plot (Fig. 23) it is clear that the visually observed gradual development of cracks created sufficiently high amplitude events but as the loading approached to the failure load a greater amount of AE hits with higher amplitudes were visible. Clearly, the trend confirms the presence of impending brittle failures. The trends in the amplitude-duration plot shown in Fig. 24 also seem to reveal that all collected AE events were from the CFRP-adhesive-concrete interface. The historic index profile (Fig. 25) reveals a gradually increasing slope of the CSS with every AE knee being corresponded to an H(I) peak. Shear failure was the failure mode of this beam and thus the historic index values are slightly low due to the quickly developing shear cracks in the concrete cross-section. The intensity chart shown in Fig. 26 also reveals the same trend of weak AE signal strength throughout the test with trends observed both visually and through parametric correlations.

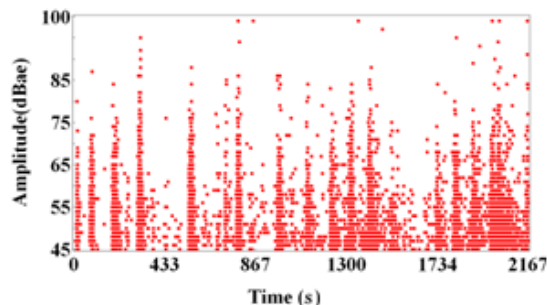


Fig. 23 Beam SM1: Amplitude vs time

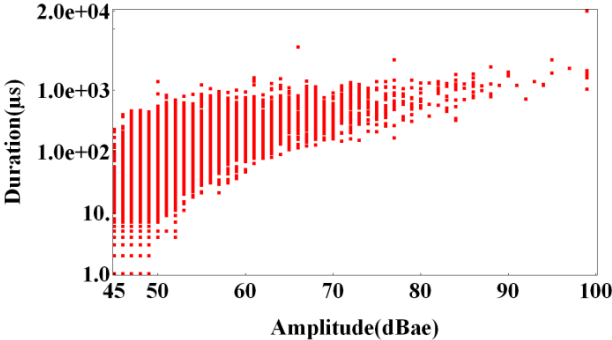


Fig. 24 Beam SM1: Amplitude vs Duration

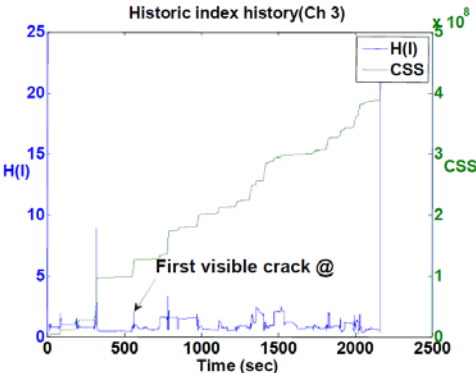


Fig. 25 Beam SM1: H(I)-CSS plot for R15I sensor

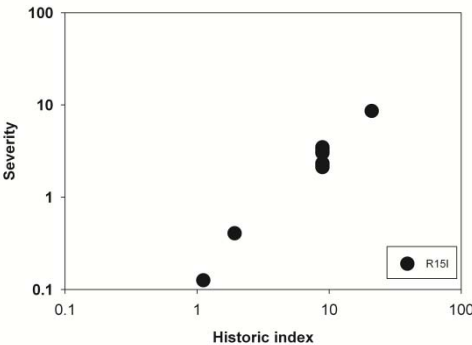


Fig. 26 Intensity chart for Beam SM1

Although from the limited number of specimens and AE channels used in the present study no standard intensity charts could be developed, an attempt is made to fit the data collected from all tested beams into a standard chart generated for FRP pressure vessels (Fowler *et al.* 1989). The data from R6I and R15I channels have been separately plotted and is shown in Figs. 27 and 28. All values in Fig. 27 are maximum intensity values from channel R6I until failure of the beam. The maximum values of three beams lie in the major damage region while one exception is noted. This point is representative of the sample that underwent shear failure in the unretrofitted region, which in turn resulted in weak AE signals being collected. Fig. 28 is from the R15I sensors located close to the midspan on the laminate surface. As mentioned previously, all sensors on the laminate were removed at about 80% of UL to prevent damage to the sensors. Thus, the maximum intensity values are significantly lower, although all specimens were tested to failure. Thus the plotted points are a good representation of the damage that is expected at that loading level.

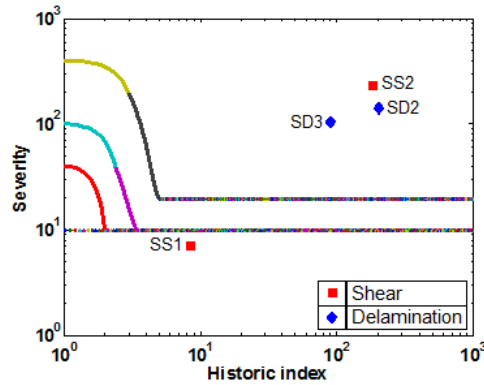


Fig. 27 Intensity chart for channel R6I in all beams

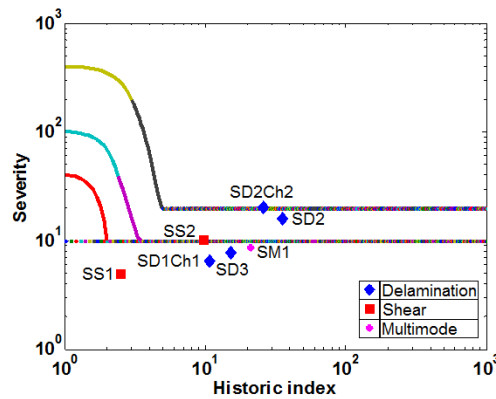


Fig. 28 Intensity chart for channel R15I in all beams

## 5. Conclusions

The results of AE monitoring of CFRP retrofitted RC beams using parametric and intensity analyses techniques were presented in this study. The objective of the tests was to monitor the change in AE parameters when the brittle failure characteristics of FRP retrofitted RC structures occur, and thus help predict similar damages in existing structures. Qualitative assessments of the structural disintegration of the retrofitted beams subjected to increased loads were made by studying the patterns generated by AE parameters such as amplitude (dB), duration and signal strength.

The parametric correlation plots illustrate that the development of flexural cracks and debonding are factors that lead sensors located on the concrete surface to collect more AE data in comparison to the AE sensor located on the laminate surface at any given instant of loading. A trend of high amplitude signals at low load levels were observed, which may be attributed to both the presence of an artificially induced flexural crack and excess resins that were used for attaching the CFRP laminate to the concrete surface. No distinct patterns were visible in the parametric correlation plots pertaining to a given failure mode. This may be due to the complex failure mechanisms involved in this structural system that involves several materials, which makes it difficult to identify individual failure mode characteristics.

A progressive tracking of historic and severity indices from each AE channel at each load step representing the decreased structural integrity of the tested beam was plotted in the intensity charts. As the damage progressed in the beam the intensity values were observed to move gradually from the lower left corner of the chart to the upper right corner.

In all, AE was an effective non-destructive monitoring tool that can trace the failure progression in RC beams retrofitted with CFRP. However, the parametric investigation is very limited and thereby the conclusion is preliminary. It would be advantageous to isolate signals originating from the CFRP and concrete, leading to a more clear understanding of the progression of the brittle damage mechanism involved in such a structural system. For practical applications future studies should focus on spectral analysis of AE data from broadband sensors and automated pattern recognition tools to classify and better correlate AE parameters to failure modes observed.

## References

- Ansari, F. (2005), "Fiber optic health monitoring of civil structures using long gage and acoustic sensors", *Smart Mater. Struct.*, **14**(3), S1-S7.
- ASTM E1316-07b (2007), *Standard Terminology for Nondestructive Examinations*, ASTM International, West Conshohocken, PA.
- Buyukozturk, O. and Hearing, B. (1998), "Failure behavior of precracked concrete beams retrofitted with FRP", *J. Compos. Constr.*, **2**(3), 138 -144.
- Buyukozturk, O., Gunes, O. and Karaca, E. (2004), "Progress on understanding debonding problems in reinforced concrete and steel members strengthened using FRP composites", *Constr. Build Mater.*, **18**, 9-19.
- Casas, J.R., Ramos, G., Carrillo, S.D. and Guemes, J.A. (2002), "Intelligent repair of existing concrete structures", *Comput Aided Civ. Inf.*, **17**, 43-47.
- Cecchini, A. (2005), *Damage detection and identification in sandwich composites using neural networks*, MS Thesis, University of Puerto Rico, Mayagüez, Puerto Rico.
- Chotickai, P. (2001), *Acoustic emission monitoring of prestressed bridge girders with premature concrete*

- deterioration*, Master's thesis, University of Texas, Austin, Tx.
- Committee on Acoustic Emission from Reinforced Plastics (CARP) (1987), *Recommended practice for acoustic emission of fiberglass reinforced plastic resin (RP) tanks/vessels*, Composites Institute, Society of the Plastics Industry, New York.
- Degala, S., Rizzo, P., Ramanathan, K. and Harries, K.A. (2008), "Acoustic emission monitoring of CFRP reinforced concrete slabs", *Constr. Build. Mater.*, **23**(5), 2016-2026.
- Fowler, T.J., Blessing, J.A. and Conlisk, P.J. (1989), "New directions in testing", *Proceedings of the 3rd International Symposium on Acoustic Emission from Composite Materials*, Paris, France, July.
- Fowler, T.J., Blessing, J.A. and Strauser, F.E. (1992), "Intensity analysis", *Proceedings of the 4th International Symposium on Acoustic Emission from Composite Materials*, American Society for Nondestructive testing, Columbus Ohio.
- Ghorbanpoor, A. and Rentmeester, A.T. (1993), "NDE of steel bridges by Acoustic emission", *Proceedings of the Structural Engineering in Natural Hazards Mitigation*, ASCE, Irvine, California, April.
- Golaski, L., Gebiski, P. and Ono, K. (2002), "Diagnostics of reinforced concrete bridges by acoustic emission", *JAE*, **20**, 83-98.
- Gostautas, R.S., Ramirez, G., Peterman, R.J. and Meggers, D. (2005), "Acoustic emission monitoring and analysis of Glass Fiber-reinforced composites bridge decks", *J. Bridge Eng.- ASCE*, **10**(6), 713-721.
- Henkel, D.P. and Wood, J.D. (1991), "Monitoring concrete reinforced with bonded surface plates by the acoustic emission method", *NDT & E Int.*, **24**(5), 139-147.
- Johnson, D.E., Shen, H.W. and Finlayson, R.D. (2001), "Acoustic emission evaluation of reinforced concrete bridge beam with graphite composite laminate", *Smart Struct. Mater.*, **4330**, 498-504.
- Lau, K.T., Yuan, L.B., Zhou, L.M., Wu, J.S. and Woo, C.H. (2001), "Strain Monitoring in FRP Laminates and Concrete Beams Using FBG Sensors", *Compos. Struct.*, **51**, 9-20.
- Levar, J. and Hamilton, H. (2003), "Nondestructive evaluation of carbon fiber-reinforced polymer-concrete bond using infrared thermography", *ACI Mater. J.*, **100**(1), 63-72.
- Mirmiran, A., Shahawy, M., and El Echary, H. (1999), "Acoustic emission monitoring of hybrid FRP-concrete columns", *J. Eng. Mech. - ASCE*, **125**(8), 899-905.
- Mirmiran, A. and Wei, Y. (2001), "Damage assessment of FRP-encased concrete using ultrasonic pulse velocity", *J. Eng. Mech. -ASCE.*, **127**(2), 126-135.
- Mirmiran, A. and Philip, S. (2000), "Comparison of acoustic emission activity in steel-reinforced and FRP-reinforced concrete beams", *Constr. Build Mater.*, **14**(6), 299-310.
- Ohtsu, M., Uchida, M., Okamoto, T. and Yuyama, S. (2002), "Damage Assessment of reinforced concrete beams qualified by Acoustic emission", *ACI Struct. J.*, **99**(4), 411-417.
- Park, J.Y., Cho, H.D., Han, H.S. and Choi, M.Y. (2004), "Detection of crack source location on RC structures strengthened with CFRP plate for health monitoring system", *Key Eng. Mat.*, **270-273**, 1971-1976.
- Ridge, A.R. and Ziehl, P.H. (2006), "Evaluation of strengthened reinforced concrete beams: cyclic load test and acoustic emission methods", *ACI Struct. J.*, **103**(6), 832-841.
- Teng, J.G., Chen J.F., Smith, S.T. and Lam, L. (2001), *FRP-strengthened RC Structures*, John Wiley & Sons, U.K.
- Whitten, L.S., Joel P., Conte and Eric, U. (1999), "Long gage fiber fragg grating sensors to monitor civil structures", *SPIE*, **4330**, 56-65.
- Yuyama, S., Okamoto, T., Shigeishi, M., Ohsu, M. and Kishi, T. (1999), "A proposed standard for evaluating structural integrity of Reinforced Concrete Beams by Acoustic emission", *Acoustic emission: Standards and Technology update*, ASTM STP 1353, (Ed. S.J. Vahaviolos), American Society for testing and materials, West Conshohocken, PA.